Published in final edited form as:
J Am Chem Soc. 2008 November 26; 130(47): 15916–15926. doi:10.1021/ja804088j.

Controlling Film Morphology in Conjugated Polymer:

Fullerene Blends with Surface Patterning

Lee Y. Park[*,‡], **Andrea M. Munro**[§], and **David S. Ginger**[*,§]

[*]*Department of Chemistry, Williams College, Williamstown, MA 01267*

§*Department of Chemistry, University of Washington, Seattle, Washington 98195-1700*

‡*Department of Chemistry, Williams College. Phone: (413) 597-2191; Fax: (413) 597-4113; E-mail: lpark@williams.edu*

§*Department of Chemistry, University of Washington, Seattle. Phone: (206) 685-2331; Fax: (206) 685-8665: E-mail: ginger@chem.washington.edu*

Abstract

We study the effects of patterned surface chemistry on the microscale and nanoscale morphology of solution-processed donor/acceptor polymer-blend films. Focusing on combinations of interest in polymer solar cells, we demonstrate that patterned surface chemistry can be used to tailor the film morphology of blends of semiconducting polymers such as poly-[2-(3,7-dimethyloctyloxy)-5-methoxy-p-phenylenevinylene] (MDMO-PPV), poly-3-hexylthiophene (P3HT), poly[(9,9-dioctylflorenyl-2,7-diyl)-*co*-benzothiadiazole)] (F8BT), and poly(9,9-dioctylfluorene-co-bis-N,N'-(4-butylphenyl)-bis-N,N'-phenyl-1,4-phenylendiamine) (PFB) with the fullerene derivative, [6,6]-phenyl-C_{61}-butyric acid methyl ester (PCBM). We present a method for generating patterned, fullerene-terminated monolayers on gold surfaces, and use microcontact printing and Dip-Pen Nanolithography (DPN) to pattern alkanethiols with both micro- and nanoscale features. After patterning with fullerenes and other functional groups, we backfill the rest of the surface with a variety of thiols to prepare substrates with periodic variations in surface chemistry. Spin coating polymer:PCBM films onto these substrates, followed by thermal annealing under nitrogen, leads to the formation of structured polymer films. We characterize these films with Atomic Force Microscopy (AFM), Raman spectroscopy, and fluorescence microscopy. The surface patterns are effective in guiding phase separation in all of the polymer:PCBM systems investigated, and lead to a rich variety of film morphologies that are inaccessible with unpatterned substrates. We demonstrate our ability to guide pattern formation in films thick enough of be of interest for actual device applications (up to 200 nm in thickness) using feature sizes as small as 100 nm. Finally, we show that the surface chemistry can lead to variations in film morphology on length scales significantly smaller than those used in generating the original surface patterns. The variety of behaviors observed and the wide range of control over polymer morphology achieved at a variety of different length scales have important implications for the development of bulk heterojunction solar cells.

lpark@williams.edu, ginger@chem.washington.edu

Supporting Information Available

NMR and MS data for **2**; full ToF-SIMS (PCA) images of patterned surfaces; brightfield optical microscopy images for all of the films; AFM images of thick MDMO-PPV films on DPN patterned surfaces; AFM topography images for P3HT:PCBM samples prepared with different annealing times; AFM topography images for P3HT;PCBM samples of different composition; Raman and fluorescence spectra of MDMO-PPV, F8BT, and PCBM; AFM, Raman, fluorescence data for polyfluorene:PCBM samples; tables summarizing the behaviors observed for all of the samples prepared. This material is available free of charge via the Internet at http://pubs.acs.org.

Introduction

The active layer in bulk heterojunction (BHJ) polymer solar cells is typically composed of a thin phase-separated film of a semiconducting polymer mixed with a soluble fullerene derivative; some commonly used materials are shown in Figure 1. The microscopic phase separation that arises between the interpenetrating donor (polymer) and acceptor (PCBM) networks in these films plays a critical role in device performance. The ideal architecture is one in which light is absorbed efficiently, while at the same time minimizing the opportunities for exciton and free carrier recombination, thereby simultaneously optimizing charge generation, separation, and transport. Various length scales are thought to be important in optimizing these different aspects of device performance. Optimal light absorption requires a relatively thick polymer layer (on the order of at least 100 nm), while charge separation requires a high interfacial area between the donor and acceptor components, with domain sizes comparable to the exciton diffusion length (~10 nm) in order to minimize exciton recombination. Optimal charge transport requires highly conductive pathways of each material (implying well-ordered domains) running through the device; it is known that transport and recombination vary dramatically with morphology across a wide range of length scales.[1-3] Given the need to balance charge generation and transport, phase separation significantly larger than the exciton diffusion length is sometimes required for optical performance. [1]

The interpenetrating networks in BHJ films arise from non-equilibrium structures formed during solution processing, and their formation is thus highly sensitive to specific deposition parameters. The choice of solvent used in spin-coating,[4-6] evaporation rate,[7,8] annealing conditions,[9-12] and use of additives[13,14] all have a profound effect on both film morphology and device performance. Typically, improved performance is attributed to alteration of the average domain size and the degree of order within individual domains. Realization of the importance of these types of parameters has led to significant improvements in device efficiency in recent years. However, a more thorough understanding of the details of the morphologies in successful devices and how they arise is still the subject of much investigation.[3,15,16] Thus the ability to control and dictate the phase separation in a more concerted and precise fashion in these films is of critical importance to improve device performance.

It is well-known that phase separation in polymer blends is governed in part by the surface energy of the underlying substrate, and that patterning a surface in order to produce a periodic variation in the surface energy can be used to template lateral periodicity in a polymer blend film. Microcontact printing (μCP) and control of surface chemistry have been used to guide both the lateral[17-19] and vertical phase separation[20] in a variety of polymer blends. Control and patterning of surface energies have been used to improve light outcoupling via grating effects in polymer light-emitting diodes,[21,22] efficiency in vertically separated photodiodes,[23,24] and air-stability of thin-film transistors.[23,25] Our group has recently demonstrated that Dip-Pen Nanolithography (DPN) can be used to template polymer film morphology in blends of polystyrene:P3HT and polystyrene:poly(2-vinylpyridine) blends down to a size range of 150 nm.[16,26] However, despite the accepted impact of nanoscale film morphology on the performance of bulk heterojunction polymer solar cells, there has been relatively little research into the effect of chemically patterned surfaces on the phase separation of polymer:fullerene blends.

In this manuscript we present a method for patterning C_{60} monolayers and then study the use of surface patterns generated via both μCP and DPN as a way of controlling film morphology in polymer:PCBM blends. We study blends of PCBM with many classes of conjugated polymers including alkoxy-PPV, polythiophene, and different polyfluorene-based copolymers. We demonstrate that both patterned C_{60} monolayers and patterned carboxylic-acid-terminated monolayers can be used to produce a rich variety of film morphologies by tailoring the chemical

contrast between the pattern and the background. We show that surface chemistry can be used to modulate film morphology and even template pattern formation in films thick enough to be of interest in actual device applications (we have studied films as thick as 200 nm) over a wide range of length scales, with surface features ranging from microns to ~100 nm in size. These length scales may be useful for studies of both transport and optical grating effects in future work. Furthermore, we show that patterned surface chemistry can affect film morphology on length scales that are smaller than the lateral dimensions of the monolayer surface patterns,[27,28] which may eventually enable us to approach length scales relevant to studies of charge separation.

Results and Discussion

Fullerene Patterned Surfaces

Our first objective was to generate patterned fullerene monolayers using the reagents and method outlined in Figure 2. Our standard approach is to generate a mercaptohexadecanoic acid (MHA) pattern on a gold surface using microcontact printing. We then react the MHA pattern with the easily prepared amine-terminated fullerene **3**, (Scheme 1) by bringing a flat (featureless) stamp inked with **3** into contact with the MHA-patterned gold surface (alternatively, the functionality of the chemical species on the surface and the stamp can be reversed: in this case fullerene carboxylic acid is printed onto a surface with a pattern of MUAm on Au). After introduction of the fullerene species, the rest of the Au surface is then backfilled with one of the thiols shown in Figure 2. This approach allows us to pattern both large and small feature sizes, as well as to vary the surface chemistry by choosing different thiols in the backfilling step. The fullerene coupling reaction takes advantage of the fact that microcontact printing can be used to form covalent linkages to the terminal groups of thiols on Au, even for reactions that normally require higher temperatures or the presence of catalysts; presumably the pre-organization of the reagents on the PDMS stamp, along with the high concentration of reactants compared with a typical solution reaction, are responsible for the relative ease of bond formation.[29-31] In both methods employed here, printing times of ~60 minutes, with gentle heating (40 °C) give rise to surfaces cleanly patterned with fullerenes. We found that we could also print fullerene itself (unsubstituted C_{60}) directly onto MUAm SAMs under similarly mild conditions (in comparison with the overnight reflux in toluene or chlorobenzene reported for the reaction of fullerene in solution with an MUAm SAM.[32,33])

This process results in clean, patterned, fullerene-terminated areas on the surface. In Figure 3a we show an AFM topography image of a C_{60} patterned surface, with the corresponding height traces after each step of the patterning procedure shown in 3c. The height of the MHA patterned areas is ~ 0.75 nm relative to the bare gold surface. After reaction with **3**, the height difference between the patterned regions and the bare gold increases; after subsequent backfilling of the bare gold with MUAm, the height difference between the fullerene patterned regions and the background areas decreases. Figure 3b shows a time-of-flight secondary ion mass spectrometry (ToF-SIMS) map of C_{60}^+ ion yield of the same pattern which clearly confirms the presence of a C_{60} pattern on the surface.

Polymer:PCBM Films on Patterned Surfaces

After successfully generating fullerene-patterned surfaces, we used microcontact printing to screen the effects of both fullerene-terminated and acid-terminated patterns (MHA with no fullerene on top) on the morphology of a series of spin-coated and annealed conjugated polymer:PCBM blends. To further tailor the contrast in surface chemistry, we employed a range of different thiols to backfill the unpatterned regions of the gold surfaces. In brief, we produced patterns with fullerene or MHA, and backfilled the surfaces with a range of different thiols (MUAm, HSpyr, MUO, BZT, and MHA, whose structures are shown in Fig. 2.) We then

spin-coated polymer:PCBM blends onto these surfaces and annealed them under flowing nitrogen. The polymers studied include poly-[2-(3,7-dimethyloctyloxy)-5-methoxy-p-phenylenevinylene] (MDMO-PPV), poly-3-hexylthiophene (P3HT), poly[(9,9-dioctylflorenyl-2,7-diyl)-*co*-benzothiadiazole)] (F8BT), and poly(9,9-dioctylfluorene-co-bis-N,N'-(4-butylphenyl)-bis-N,N'-phenyl-1,4-phenylendiamine) (PFB). The complete range of polymer:PCBM and pattern/backfill combinations investigated is summarized in Table 1. Except where otherwise indicated, the microcontact-printed surface patterns consisted of a square array of circular MHA or fullerene features (2.0 or 2.2 microns in diameter depending on the stamp used) on a 4 micron pitch (center-to-center) in a background of the backfill thiol. The weight ratio of polymer to PCBM, the solvent chosen, and the annealing conditions varied with the polymer, and were selected to be reasonably representative of the composition and processing conditions commonly used for devices in each polymer system. These parameters are also included in Table 1.

Interestingly, the majority of the polymer:PCBM and pattern/backfill combinations led to film morphologies that were distinctly different from those obtained by spin-coating and annealing the polymer:PCBM blends on unpatterned substrates. Figures 4 and 5 provide a summary of AFM topography images for the full range of films studied. It is clear that surface patterning was successful in controlling the overall polymer film morphology in all four of the polymer:PCBM systems studied. Furthermore, the nature of the film morphology within each family varies dramatically depending on the combination of pattern and backfill used. As can be seen from Figs. 4 and 5, fullerene terminated monolayers provide an effective means of altering film morphology in many polymer:PCBM blends. Though we initially expected that PCBM would preferentially aggregate on regions of the substrates derivatized with C_{60}, this was not always the case. We also found that substrates patterned with only non-fullerene species could also be effective in guiding phase separation in all of the polymer:PCBM mixtures (though generally leading to different film morphologies from that of the fullerene-patterned substrates). The observed behaviors were entirely reproducible, with the exception of patterns involving MUAm as the backfill reagent, which proved to be somewhat less consistent overall. The majority of the observed contrast was obtained during the thermal annealing step. Prior to annealing, the films were topographically uniform, with only modest variation in film thickness (~1 nm) giving any indication of the underlying surface pattern. After annealing, no further changes in morphology were observed for any of the films after storing at RT under ambient conditions for periods up to several months. We describe the results for each polymer:PCBM system in greater detail below; a tabular summary of the behaviors observed for all of the different types of polymer films is provided in the Supplemental Information (Tables S1-S4).

MDMO-PPV:PCBM Films on Microcontact Printed Surfaces

Figure 4a-i show the AFM topography images for MDMO-PPV:PCBM films spin-coated on the entire family of pattern/backfill combinations that we studied (corresponding optical brightfield images are shown in supporting information Figure S8). Some combinations of pattern and backfill (C_{60}/MUAm, C_{60}/MUO, C_{60}/MHA, MHA/MUAm) give rise to aggregation of material on the patterned areas (circles) resulting in elevated topography, while the remaining combinations lead to a relative depletion of material on the patterned regions of the substrate and a corresponding decrease in film thickness in those regions. In those samples where material has been depleted from the patterned areas, the effect appears to be the greatest at the perimeter of the patterned areas, with the formation of clumps of material at the centers. The development of the large topographic features across the surface of the film indicates that lateral migration of material is very pronounced in these samples.

Spatial Variation in Composition of Films

We studied the lateral composition of the samples by means of Raman spectral mapping and fluorescence imaging. Fullerenes have a distinctive Raman signal at ~1460 cm^{-1}, which is easily distinguished from signals due to MDMO-PPV, and could therefore be used to generate line scans of PCBM intensity across the films. In some cases the correlation between intensity of the Raman signal and the AFM image was clear, while in other cases no clear periodic variation in the Raman signal intensity could be detected. It should be noted that since the Raman analysis probes the entire film depth, the intensity of the Raman signal is dependent on the thickness of the film. Thus, variation in signal intensity must be considered carefully, remembering to account for film thickness. In a control experiment we patterned a surface with fullerene, and spin-coated an MDMO-PPV film without any PCBM on top. We were unable to detect the 1460 cm^{-1} band arising from the fullerene species used in the surface patterning, allowing us to conclude that all of the observed signal at 1460 cm^{-1} in our samples was due to the PCBM in the bulk of the film, as opposed to the relatively small amount of **3** introduced onto the surface by the microcontact printing process. Fluorescence imaging of these samples was carried out by excitation with a 632 nm laser; at this wavelength, there is no photoluminescence from the MDMO-PPV, but there is a clear feature centered at ~725 nm due to PCBM photoluminescence. The intensity of PCBM photoluminescence is not a measure of PCBM concentration, but of PCBM that has aggregated into crystallites large enough that their photoluminescence is not efficiently quenched by the polymer.[6] Just as in the Raman spectroscopy experiments, we found that we could not detect photoluminescence from the microcontact printed layer of **3**, allowing us to conclude that all of the ~725 nm fluorescence came from the bulk of the film. The combination of AFM, Raman, and fluorescence data, along with comparisons among samples, allowed us to draw conclusions about the nature of the lateral distribution of PCBM and polymer in the different films. Both Raman and fluorescence data indicate the presence of PCBM throughout all regions of all these films. In other words, the phase segregation gives rise to regions that are enriched or depleted in one component or the other, but that are not pure (given the lateral and vertical resolution of the methods employed here). This result is consistent with previous studies of polymer:fullerene and polymer:polymer phase segregation.[34,35] The large variation in the behavior of films on substrates with different surface chemistries is indicative of a complex interplay between the interfacial energies of the pattern, backfill, polymer, and PCBM. Because of these variations in behavior, we will not try to describe every sample in detail. Instead we present examples representing a range of observed behaviors below (a more complete summary of these results can be found in Table S1.)

Figure 6 compares the AFM topography, Raman line scans, and fluorescence images obtained for annealed MDMO-PPV:PCBM films cast onto five different types of substrates: C_{60}/MHA, C_{60}/MUO MHA/BZT, MHA/HSpyr, and MHA/MUAm. A comparison of 6a and 6b serves to illustrate the surprising and reproducible variations in behavior observed for substrates with what we considered to be similar surface chemistries. For the C_{60}/MHA sample (6a), AFM indicates significant aggregation of material on the C_{60}-patterned regions, with the thicker regions of the film ~3 times as thick as the background areas. The periodic variation in the intensity of the 1460 cm^{-1} Raman signal is also ~3 times stronger in the thicker areas of the film than in the thinner areas of the film, suggesting that the net composition of the thinner and thicker regions of the film is similar. However, the fluorescence image for this sample is very interesting and indicates the development of fine structure within the different areas of the film, showing bright PCBM fluorescence at the centers of the patterned areas, as well as the background of the film, but not at the edges of the patterns. This suggests clustering of the PCBM both in the background as well as the center of the patterned areas. We note that the pattern edges appear to be depleted of luminescent PCBM on a length scale much smaller than the feature size of the stamps. This finding suggests that the interface between regions of

different surface chemistry can give rise to different structures than are possible on either unpatterned surface, and to structures within the polymer films on a length scale smaller than that used in the surface patterning. By comparison, the AFM image for the polymer film on the C_{60}/MUO substrate (6b) once again indicates aggregation of material on the patterned C_{60} features. However the Raman scans and fluorescence images both show *less* fullerene signal on the C_{60} patterns than on the MUO background. Despite a film that is ~4 times thicker on the C_{60} patterned regions, the fullerene Raman signal is ~6 times weaker. These data suggest that upon annealing in this film, there is simultaneous migration of polymer towards (and PCBM away from) the patterned regions of the surface. In this case we see that luminescent clusters of PCBM have formed throughout the background areas, with a small region of luminescent PCBM at the very center of the patterned areas.

A comparison of the MHA/BZT and MHA/HSpyr samples (6c and 6d respectively) also serves to illustrate the variation in behavior for polymer films on substrates with similar surface chemistries. On both of these substrates, AFM shows the patterned areas recessed relative to the background, with some aggregation of material visible at the centers of the patterned circles, particularly for the MHA/BZT sample. However, the Raman data once again show different behavior between the two samples, despite the apparent similarity of the topographies. In the MHA/BZT sample the patterned regions exhibit an increased PCBM Raman signal on the patterned areas despite the decrease in film thickness, suggesting that polymer migration away from the patterned areas is occurring simultaneously with PCBM migration to those areas. In the MHA/HSpyr sample (6d), Raman data indicate a weaker PCBM signal in the thinner (patterned) regions of the film, suggesting that polymer movement away from the patterned regions is the primary cause of the observed variation in film thickness. (In 6c and 6d the variations in film thickness and in Raman signal intensity across the samples are considerably less pronounced than those observed in 6a and 6b.) Fluorescence microscopy indicates the formation of luminescent clusters primarily on the centers of the patterned regions. The background regions in both samples show some PL as well, confirming the presence of some aggregated PCBM throughout the films, however the lower intensity suggests that most of the PCBM in these regions remains relatively intimately mixed with polymer, and therefore does not lead to very strong fluorescence. It is clear that the surface patterns influence not only the bulk migration of the polymer and PCBM, but also the degree to which PCBM within a given region tends to aggregate into luminescent clusters.

Finally, Fig. 6e provides data for the MHA/MUAm sample. The AFM image indicates accumulation of material on the patterned regions, while the Raman line scan indicates a lower concentration of PCBM on those same regions (in spite of the greater thickness of the film.) Upon annealing there is net movement of the polymer towards the patterned regions with concurrent movement of the PCBM away from these same areas. The PCBM in the background (unpatterned) regions has a greater tendency to form more-luminescent clusters, while the PCBM that remains in the patterned regions remains more intimately mixed with the polymer. Close inspection of the fluorescence data for this sample indicates fine structure in the fluorescence image on smaller length scale than that used in the microcontact printing.

In summary, we observe changes in film morphology in all MDMO-PPV:PCBM films processed onto substrates patterned with microcontact-printed surface chemistry. The patterned chemistry can be used to produce variations in film thickness as large as 70-90 nm after annealing in films that were initially uniformly 100-120 nm thick, and can be used to enhance or diminish local PCBM concentration and the degree of nanoscopic PCBM aggregation. The interfaces between two kinds of surface chemistry can exhibit different properties from either patterned region and, intriguingly can lead to the formation of structure within the polymer:PCBM films on length scales considerably smaller than the microcontact printed patterns themselves (see also supporting information Fig. S15). Whether the observed

morphologies evolve primarily due to polymer vs. PCBM migration or a combination of the two appears to vary with each substrate. PCBM does not always prefer to aggregate on fullerene patterned regions, nor on regions derivatized with other aromatic groups. Furthermore, surfaces backfilled with different thiols that might be expected to have similar chemical properties do not always give rise to the same type of behavior. While this behavior could presumably be understood more systematically in the context of the relevant surface energies and interaction parameters, very little data of this type is available for materials used in organic electronic devices.[36,37]

MDMO-PPV:PCBM Films on DPN-Patterned Surfaces

We have demonstrated that the behavior of annealed MDMO-PPV:PCBM films on patterned surfaces is dramatically different than that observed on unpatterned substrates. Given the importance of film-morphology to device performance, these results indicate that patterned surface chemistry is a promising avenue to explore for optimizing organic solar cells. However, the relevant length scales for optimizing polymer blend solar cells are in the ~10 nm range for exciton harvesting, ~100 nm for charge collection, and ~100-1000 nm scale for light scattering. We therefore now consider the ability of sub-micron features to change the morphology in polymer films of different thicknesses, allowing us to approach some of these critical length scales.

We studied films between 50 and 200 nm in thickness on MHA/HSpyr substrates, and found that the surface-guided morphology changes occurred readily in all cases for even the thickest films studied. To study the effects of sub-micron surface features on polymer:PCBM blends that may be useful in light scattering strategies or eventually (at smaller length scales) for improved exciton harvesting and transport, we created surface patterns using DPN rather than microcontact printing. Figure 7 shows AFM images and height profiles for 100 nm thick MDMO-PPV:PCBM films spin-coated and thermally annealed on DPN-patterned (MHA/HSpyr) surfaces. In Fig. 7a-c the size of the patterned features remains constant at 200 nm while the pitch is decreased. In Fig. 7d-f the pitch is held constant at 750 nm while the feature size is decreased from 400 to 130 nm. The depressions created in the surface of the films are significantly wider at the top (the polymer/air interface) than at the bottom, which will affect how closely spaced the features can be placed before they interact. For instance, in 7c, 200 nm MHA dots are spaced 500 nm apart (an edge-to-edge separation of 300 nm). Though the individual depressions in the overlying polymer film appear to be distinct, there is some indication that the boundaries between the individual dots are beginning to merge together. Ultimately however, we find that we can get clear pattern transfer from the surface to the polymer with surface features as small as ~130 nm in diameter (7f). As the surface feature size is decreased, the depth of the recessed area in the polymer film is also decreased, which may reflect migration of a smaller volume of polymer away from the smaller patterned area. Significantly, we can achieve similar results with films close to 200 nm in thickness, suggesting that vertical/lateral aspect ratios of 2 can be achieved using only surface chemistry (Figure S11). For smaller features (we studied features down to 80-100 nm in diameter) we believe that the surface patterns still cause changes in the overlying film morphology and we can see topographic changes due to the pattern in some areas, however for the sub-100 nm features studied under these conditions we could not make out the entire perfect array of dots/columns. Nevertheless, the ability to generate features in the ~100 nm range coupled with the observation (from the fluorescence studies described above) that surface patterning can lead to fine structure on a length scale smaller than that of the surface pattern suggests that surface chemistry is worth exploring in more detail as a means for improving exciton harvesting and charge transport. Furthermore, the ready generation of 130-700 nm features using surface chemistry suggests that chemical modification of the anode could be useful for generating optical grating structures[38,39] in polymer:PCBM blend photodiodes.

P3HT:PCBM Films on Micro-Contact Printed Surfaces

As was observed for the MDMO-PPV:PCBM blends, the morphology of P3HT:PCBM blends also shows considerable sensitivity to presence of underlying surface patterns. Figs. 4j-r show clear variations in film morphology for P3HT:PCBM films spin-coated and annealed on the 9 studied combinations of pattern/backfill chemistry. Brightfield optical microscopy images also show evidence for morphological changes in several samples (supporting information Figure S8). The only samples that do not show any evidence of changes from the surface patterning are the C_{60}/MHA and the MHA/MUAm samples. Interestingly, these two combinations did show clear effects on the MDMOPPV:PCBM films (compare Figs. 4n-o with Figs. 4e-f). We were unable to make significant quantitative use of either Raman or fluorescence analysis on the P3HT:PCBM blends because P3HT has a Raman band that overlaps with the PCBM signal and also gives rise to significant PL when excited with 632 nm light. However, the shapes of the Raman and fluorescence spectra suggest that both PCBM and P3HT were present throughout all of the films, just as we found with the MDMO-PPV:PCBM samples.

Large clusters are visible in the AFM topography images in Figs. 4k, l, p, q, and r. We assign these clusters as being mostly PCBM because the density of the clusters tracks directly with the PCBM concentration, and we observe no clusters in films of pure polymer (Figure S10). Other groups have also identified similar clusters that form upon annealing P3HT:PCBM films as being PCBM domains.[11,40] As in the MDMO-PPV:PCBM system, we find surprising behavior in terms of where the PCBM appears to aggregate. For the C_{60}/HSpyr and MHA/HSpyr patterns, we observe preferential formation of PCBM clusters on the patterned C_{60} and MHA areas respectively, while for the MHA/MUO sample the PCBM aggregates form selectively on the background MUO areas rather than on the patterned MHA. For the C_{60}/BZT and MHA/BZT samples, it is difficult to relate the regions of cluster formation with the underlying surface pattern. However, having prepared similar samples using milder annealing conditions, we believe that the PCBM first aggregates in the background areas of the pattern. As the annealing proceeds, the initial clumps begin to aggregate and grow, eventually giving rise to the more elongated crystallites seen in the AFM images in Fig. 4.

P3HT:PCBM Films on DPN-Patterned Surfaces

By studying DPN-patterned surfaces with the P3HT:PCBM blends we were again able to explore the lower limits on pattern size and spacing on the phase segregation process. Figure 8a shows an AFM image for a P3HT:PCBM film on a DPN pattern (MHA/HSpyr) consisting of 6 × 6 array of ~600 nm dots with a center-to-center pitch of 1 μm annealed at 125 °C for 30 minutes. The tendency of the PCBM to form large micron-sized aggregates on many kinds of surfaces during annealing can complicate efforts to find printed patterns that have been miniaturized below the natural size of the PCBM domains. For instance, in Fig. 8a the sub-micron DPN template is obvious in the AFM topography of the polymer film, however the MHA pattern has also nucleated a number of larger PCBM aggregates which have grown well beyond the DPN sites and are beginning to obscure the underlying grid. We found that we could minimize this effect by decreasing the size of the patterned features relative to the pitch of the array. To this end, Fig. 8b shows the topography of a P3HT:PCBM film spin-coated onto an array of ~200 nm dots with a pitch of 1 μm, then annealed at 125 °C for 30 minutes. We found this template size to be about the lower limit that would consistently lead to observable grids in the P3HT:PCBM films. Altering the annealing conditions slightly also allowed us to avoid the formation of the larger PCBM aggregates: Figure 8c shows an array of 600 nm dots with a pitch of 1.25 μm annealed at 120 °C for 30 minutes, followed by annealing at 125 °C for 30 minutes. Though we were able to prevent the formation of very large clumps as seen in 8a by this means, the formation of smaller crystallites throughout the film (and the corresponding increase in surface roughness) makes it difficult to make out the changes due to these relatively large (~600 nm) features.

Polyfluorene:PCBM films

In addition to blends with MDMO-PPV and P3HT, we also studied the effects of patterned surface chemistry on film morphology with two commercially available polyfluorene copolymers, F8BT and PFB. Although these particular polymers do not make good solar cells with PCBM, a wide range of polyfluorene copolymers is currently under investigation for solar cell applications[41,42] and we wanted to study the effects of surface chemistry on examples of polymers from that family.

Figure 5a-i and Figure 5j-r show AFM topography images of ~150 nm-thick F8BT:PCBM and PFB:PCBM blends spin-coated then annealed onto a range of patterned surface chemistries. Consistent with the theme of this paper, the patterned chemistry has a clear effect on many of the film morphologies, even those where perfect pattern replication of the monolayer template by the thick polymer film is not observed. Because of the similarities in behavior between the two types of polymer, we will only discuss the F8BT:PCBM samples (Fig. 5a-i) in detail below. Though changes in the film morphologies are evident in most of Fig. 5, the topographic features of the films are not nearly as dramatic as those found in the P3HT:PCBM and MDMO-PPV:PCBM examples. However, the reduced topographic contrast should not be taken as a sign of a reduced effect of the surface template in all samples. For instance, as with the previous polymer blends, brightfield images show changes in the morphology resulting from the surface patterns in almost all of the films (supporting information Figure S9). However for these samples, the morphological changes are actually more evident in some of the optical microscopy images than they are in the corresponding AFM images. This is in contrast to the MDMO-PPV:PCBM and P3HT:PCBM films where the clarity of the patterns observed by AFM and the clarity of the patterns observed optically were generally correlated. The only polyfluorene:PCBM films for which we did not find evidence of surface-guided phase segregation in either the AFM or optical images were the PFB:PCBM samples cast onto C_{60}/MUO, C_{60}/MHA, and MHA/HSpyr substrates. We also carried out fluorescence and Raman studies on the F8BT:PCBM films (Figure S14). For the F8BT:PCBM films cast onto both the C_{60}/BZT and MHA/BZT substrates, we observed PCBM photoluminescence primarily from the patterned regions of the surface. Raman results for these two samples indicated higher concentrations of PCBM on the pattern in the case of the C_{60}/BZT, but higher concentration of PCBM in the background in the case of MHA/BZT. However, the F8BT:PCBM films cast onto C_{60}/BZT and MHA/BZT substrates were the exceptions: there was no detectable periodicity in either the fluorescence or Raman data on the other samples, despite obvious contrast in the AFM topography and optical brightfield images. These observations suggest that the nature of the phase separation may be qualitatively different in many of these systems than in the MDMO-PPV:PCBM and P3HT:PCBM samples. Although future study is needed, one possible explanation is that vertical phase segregation plays a larger role than lateral phase segregation in these polyfluorene samples.

Conclusions/Future Work

In summary, we have patterned monolayers of C_{60} and a series of alkanethiols using both μCP and DPN. We have shown that these patterned monolayers provide a powerful route for controlling film morphology in a wide range of technologically important conjugated polymer:fullerene blend films (including blends of P3HT, MDMO-PPV, PFB, and F8BT with PCBM). Depending on the polymer and surface chosen, the patterns can increase or decrease the concentration of the polymer or PCBM, and can lead to preferential formation of PCBM clusters in certain areas. In addition to micron-scale features generated with μCP, we have used DPN to show that features as small as 130 nm can guide phase separation in films ~ 200 nm thick. Furthermore, we observe that the patterned monolayers can alter the morphology of the film significantly even when the polymer does not appear to follow the surface pattern, and

that surface chemical patterns can cause changes in film morphology on length scales significantly smaller than the dimensions of the patterned features. Our results demonstrate that surface patterning may provide the means for improving various aspects of device performance, from the inclusion of grating structures (length scales of hundreds of nm) to charge recombination and transport (tens to hundreds of nm), and with future work, may even reach the scale of the exciton diffusion length (~10 nm) by exploiting interracial effects between patterned areas. While much work remains to be done to understand the details of how particular surface chemistry combinations achieve specific morphological results, it is clear that seemingly small changes in surface chemistry can have a large impact on the resulting film morphology, leading to very different behaviors even for surface chemistries with similar surface chemistries; this suggests that the interplay between the different interfacial energies involved is more complex than one might intuitively suspect, and should motivate future studies of interactions between organic semiconductors and monolayer-functionalized surfaces. Surface roughness (differences in height based on the pattern vs. backfill components) may also play a role in determining the evolution of the morphology in some of these films.[43] In spite of the fact that we don't yet understand how all of these factors interact to give rise to different film structures, it is evident that variation in the surface chemistry provides very fine control over the nature of the final film morphology.

The effect of film morphology on the performance of polymer LEDs and photodiodes is well known, however, with a few exceptions[13,44-47] most research to date has focused on optimizing device performance through the choice of solvent and post-processing such as thermal or solvent annealing. Our results suggest that patterned surface chemistry could provide another general tool that should be more fully explored to optimize both lateral[11] and vertical[23,24] film morphology to improve device performance via light trapping approaches[38,39,48] or even through improved exciton harvesting and charge collection. While DPN is a useful technique for screening the effects of nanoscale features on the morphology of semiconducting polymer films in the lab, the generation of microscale and nanoscale chemical features using methods compatible with the roll-to-roll processing techniques proposed for polymer solar cells should also be possible.

Experimental

General Procedures

C_{60}, fullerene carboxylic acid, mercaptohexadecanoic acid (MHA), mercaptoundecanol (MUO), benzenethiol (BZT), and mercaptopyridine (HSpyr) were purchased from Aldrich Chemicals. Mercaptoundecylamine (MUAm) was purchased as the hydrochloride salt from Dojindo Chemicals. PCBM was purchased from Nano-C and P3HT from Rieke Metals. F8BT and PFB were purchased from American Dye Source. MDMO-PPV was synthesized by the Gilch route.[49] Thermally oxidized Si wafers (10,000 Å, 100, Wafer World), 99.999% gold pellets from K. J. Lesker, and chromium-coated tungsten rods (Midwest Tungsten Service) were used in the preparation of gold surfaces for patterning.

NMR spectra were taken on a Bruker 500 MHz Avance Spectrometer. Thermal annealing was carried out on a Linkam LTS350 heating stage, under flowing N_2. AFM imaging and DPN patterning were carried out under ambient conditions on either a Dimension 3100 or an Asylum MFP-3D system. Raman spectra and line scans were taken on a Renishaw InVia system equipped with an inverted Leica DMIRBE microscope; all spectra and scans were taken using a 50x objective, with 785 nm laser excitation, with 3-4 sec acquisition time. For fluorescence studies, the polymer blend samples were imaged using a 50X objective (L Plan 50X) in epi-illumination geometry on a Nikon TE2000-U inverted microscope. The samples were excited with a HeNe cw laser (Melles Griot 05-LHP-121) and passed through a 25 nm bandpass filter centered at 630 nm (Comar 630 IL 25). The laser beam was defocused with a convex lens (focal

length = 125 mm) prior to entering the microscope objective. The power density at the sample surface was ~480 W*cm^{-2}. The sample photoluminescence was collected by the objective and passed through a 50/50 beam splitter and passed through a 80 nm bandpass filter centered at 740 nm to block scattered laser light (Chroma OSO2617 D740/80x). Finally the light was collected by a Roper Scientific liquid nitrogen cooled CCD (Spec-10:400B/LN). Images were collected with a 200 msec integration time, an analog to digital converter speed of 2 MHz, and a gain setting of 2 (corresponding to 8 detected electrons per A/D units generated). The image area of each pixel corresponded to an area of 0.16 μm^2. ToF-SIMS experiments were performed using a ToF-SIMS V from Ion-ToF GmbH (Munster, Germany). A 25 keV pulsed Bi_3^+ beam was raster-scanned across the target and secondary ion images of the micropatterned sample were obtained by plotting the intensity of the selected ions with respect to the coordinates of the beam on the target. The primary ion dose was kept under static conditions during all experiments (<10^{12} ions/cm^2). The beam was operated in the high current unbunched mode (lateral resolution around 1 μm and unit mass resolution) and hit the target at an angle of 45°.

Synthesis of **3,** (6,12,15,18-tetra-(4-aminopiperidin-1-yl)-6,12,15,18-(tetrahydro)oxireno [2′, 3′:1,9] (C_{60}-I_h)-[5,6]fullerene **1**[50] (0.49 g, 3.24 × 10^{-4} mol) was dissolved in 25 mL CH_2Cl_2, 3 mL TFA was added, and the solution was stirred at room temperature for 4 hours. The solvent was removed in vacuo, giving **2** as a red-brown oil. **2** was then suspended in 20 mL chlorobenzene and 3 mL NEt_3 were then added to the flask and stirred for 3 hours, giving an orange-red solution of **3**, which was used directly in the inking of PDMS stamps for patterning, as described below. The solutions were typically used for several weeks.

^{1}H NMR of **2** (500 MHz, d_6-DMSO): 1.71 (m, 8H), 2.10 (m, 8H), 2.90 (m 8H), 3.25 (m 4H), 3.60 (m 8H), 8.15 (m, 12H). ^{13}C NMR of **2** (500 MHz, d_6-DMSO): 29.02, 30.15, 30.31, 47.07, 47.36, 47.60, 48.09, 48.72, 49.05, 70.99, 71.37, 74.93, 76.07, 115.91 (q, $^1J_{CF}$ = 292 Hz, CF_3),137.8, 140.18, 142.46, 142.60, 142.99, 143.24, 143.41, 143.58, 144.12, 144.29, 144.79, 144.88, 145.90, 146.46, 146.56, 146.69, 146.77, 147.01, 147.19, 147.31, 148.67, 148.90,158.56 (q, $^2J_{CF}$= 36 Hz, CCF_3). ESI-MS of **2**: Mass expected for $C_{80}H_{44}N_8O$ (four trifluoroacetic acids units are removed in the ionization process): 1133.75; found: 1133.7.

Patterned surfaces

Patterned surfaces were prepared by first cleaning Si via sonication in acetone and isopropyl alcohol for 15 minutes each. Immediately following cleaning, 25-30 nm films of gold were prepared by thermal evaporation (Auto 306, Edwards) onto a 2-3 nm Cr adhesion layer. Gold surfaces were used within a few hours of preparation. All solutions used were 1 mM in absolute EtOH, unless otherwise specified.

Fullerene patterned surfaces—A pattern of MHA (or MUAm) was prepared on a fresh gold surface either via DPN or μCP (2 minutes, RT.) (In cases where MUAm was used, after patterning, the sample was soaked in a 1:10 v:v solution of NEt_3 in EtOH for 15 seconds before proceeding.) The sample was then rinsed with ethanol and dried under N_2. A flat (featureless) PDMS stamp was then inked with a solution of **3** (or fullerene carboxylic acid) and dried. The stamp was brought into contact with the patterned surface for 45-60 minutes with gentle pressure at a temperature of 40 °C. The sample was then sonicated in chlorobenzene for 1 minute, rinsed thoroughly with EtOH, and dried under N_2. The surface was then backfilled by soaking in a solution of the appropriate thiol for 2 minutes, followed by rinsing with EtOH, and drying under N_2. In the case of mercaptoundecylamine (MUAm) backfill, following soaking in a solution of the hydrochloride salt, the samples were dipped in a 1:10 (v:v) solution of NEt_3 in EtOH for 15 seconds, followed by rinsing with EtOH and drying under N2. DPN tips for writing with MHA were prepared by dipping silicon nitride probes (Veeco, MSCT-AUHW, force constant = 0.05 N/m) in a saturated solution of MHA in EtOH for 20 seconds.

The tips were then exposed to water vapor for 2 minutes, and dipped into the saturated MHA solution for a further 20 seconds, followed by drying under a stream of N_2

MHA patterned surfaces—These surfaces were prepared exactly as described above, except that the step involving the microcontact printing of the fullerene species was omitted.

Polymer:PCBM Films—Polymer:PCBM solutions and films were prepared as described below (except where indicated.) All solutions were filtered through a 0.3 micron PTFE filter (Pall Life Sciences) prior to spin-coating (WS-400B-6NPP/LITE from Laurell Technologies.)

MDMO-PPV:PCBM solutions were prepared in chlorobenzene (1:4 w:w) with a polymer concentration of 5 mg/mL. After spin-coating (3 seconds at 300 rpm, 2 minutes at 2400 rpm, 30 seconds at 5000 rpm) onto patterned surfaces, films (~100 nm thick) were annealed at 80 °C for 8 hours under N_2.

P3HT:PCBM solutions were prepared in chlorobenzene (1:2 w:w) with a polymer concentration of 10 mg/mL. After spin-coating (3 seconds at 300 rpm, 2 minutes at 2400 rpm, 30 seconds at 5000 rpm) onto patterned surfaces, the films (~ 60 nm thick) were annealed at 130 °C for 30 minutes under N_2.

F8BT:PCBM and PFB:PCBM solutions were prepared in chloroform (1:2 w:w) with a polymer concentration of 12 mg/mL. After spin-coating (3 seconds at 300 rpm, 2 minutes at 1900 rpm, 30 seconds at 5000 rpm) onto patterned surfaces, films (~120 nm thick) were annealed at 100 °C for 1 hour under N_2.

Supplementary Material

Refer to Web version on PubMed Central for supplementary material.

Acknowledgements

Some of this work was conducted at the Nanotech User Facility at the University of Washington, a member of the National Nanotechnology Infrastructure network (NNIN) supported by NSF with assistance from Qiuming Yu and Paul Wallace. The surface analysis experiments were done at NESAC/BIO and were supported by the NIBIB grant EB-002027 with assistance from Jeremy Brison and Roger Michel. L.Y.P. acknowledges support from NSF RUI-0415437. D.S.G. and A.M.M. acknowledge support from NSF (DMR-0120967 and DMR-0449422) and from the Air Force Office of Scientific Research. D.S.G. also thanks the Camille Dreyfus Teacher-Scholar Awards Program for support. D.S.G. is a Cottrell Scholar of the Research Corporation, and an Alfred P. Sloan Foundation Research Fellow.

References

(1). McNeill CR, Westenhoff S, Groves C, Friend RH, Greenham NC. J. Phys. Chem. C 2007;111:19153–19160.

(2). van Duren JKJ, Yang X, Loos J, Bulle-Lieuwma CWT, Sieval AB, Hummelen JC, Janssen RA. J. Adv. Funct. Mater 2004;14:425.

(3). Coffey DC, Reid OG, Rodovsky DB, Bartholomew GP, Ginger DS. Nano Lett 2007;7:738–744. [PubMed: 17295549]

(4). Liu J, Shi Y, Yang Y. Adv. Funct. Mater 2001;11:420–424.

(5). Shaheen SE, Brabec CJ, Sariciftci NS, Padinger F, Fromherz T, Hummelen JC. Appl. Phys. Lett 2001;78:841.

(6). Hoppe H, Niggeman M, Winder C, Kraut J, Hiesgen R, Hinsch A, Meissner D, Sariciftci NS. Adv. Funct. Mater 2004;14:1005–1011.

(7). Li G, Yao Y, Yang H, Shrotriya V, Yang G, Yang Y. Adv. Funct. Mater 2007;17:1636–1644.

(8). Mihailetchi VD, Xie H, de Boer B, Popescu LM, Hummelen JC, Blom PWM, Koster LJA. Appl. Phys. Lett 2006;89:012107.

(9). Nguyen LH, Hoppe H, Erb T, Günes S, Gobsch G, Sariciftci NS. Adv. Funct. Mater 2007;17:1071–1078.

(10). Li G, Shrotriya V, Yao Y, Yang Y. J. Appl. Phys 2005;98:043704.

(11). Campoy-Quiles M, Ferenczi T, Agostinelli T, Etchegoin PG, Kim Y, Anthopoulos TD, Stavrinou PN, Bradley DDC, Nelson J. Nature Mat 2008;7:158–164.

(12). Zhong H, Yang X, deWith B, Loos J. Macromolecules 2006;39:218–223.

(13). Peet J, Kim JY, Coates NE, Ma WL, Moses D, Heeger AJ, Bazan GC. Nature Mat 2007;6:497.

(14). Sivula K, Ball ZT, Watanabe N, Fréchet JMJ. Adv. Mater 2006;18:206–210.

(15). Yang X, Loos J. Macromolecules 2007;40:1353–1362.

(16). Coffey DC, Ginger DS. J. Am. Chem. Soc 2005;127:4564–4565. [PubMed: 15796508]

(17). Böltau M, Walheim S, Mlynek J, Krasch G, Steiner U. Nature 1998;391:877–879.

(18). Karim A, Slawecki TM, Kumar SK, Douglas JF, Satija SK, Han CC, Russell TP, Liu Y, Overney R, Sokolov J, Rafailovich MH. Macromolecules 1998;31:857–862.

(19). Raczkowska J, Cyganik P, Budkowski A, Bernasik A, Rysz J, Raptis I, Czuba P, Kowalski K. Macromolecules 2005;38:8486–8493.

(20). Arias AC. J. Macromol. Sci. C, Polym. Rev 2006;46:103–125.

(21). Corcoran N, Ho PKH, Arias AC. Appl. Phys. Lett 2004;85:2965–2967.

(22). Fichet G, Corcoran N, Kho PKH, Arias AC, MacKenzie JD, Huck WTS, Friend RH. Adv. Mater 2004;16:1908–1912.

(23). Arias AC, Corcoran N, Banach M, Friend RH, MacKenzie JD, Huck WTS. Appl. Phys. Lett 2002;80:1695–1697.

(24). Corcoran N, Arias AC, Kim JS, MacKenzie JD, Friend RH. Appl. Phys. Lett 2003;82:299–301.

(25). Salleo A, Arias AC. Adv. Mater 2007;19:3540.

(26). Wei JH, Coffey DC, Ginger DS. J. Phys. Chem. B 2006;110:24324–24330. [PubMed: 17134183]

(27). Cheng JY, Rettner CT, Sanders DP, Kim H-C, Hinsberg WD. Adv. Mater 2008;20:3155–3158.

(28). Kargupta K, Sharma A. Langmuir 2003;19:5153–5163.

(29). Sullivan TP, van Poll ML, Dankers PYW, Huck WTS. Angew. Chem. Int. Ed 2004;43:4190–4193.

(30). Rozkiewicz DI, Jánczewski D, Verboom W, Ravoo BJ, Reinhoudt DN. Angew. Chem. Int. Ed 2006;45:5292–5296.

(31). Rozkiewicz DI, Ravoo BJ, Reinhoudt DN. Langmuir 2005;21:6337–6343. [PubMed: 15982040]

(32). Chen K, Caldwell WB, Mirkin CA. J. Am. Chem. Soc 1993;115:1193–1194.

(33). Sahoo RR, Patnaik A. Journal of Colloid and Interface Science 2003;268:43–49. [PubMed: 14611770]

(34). McNeill CR, Watts B, Thomsen L, Belcher WJ, Greenham NC, Dastoor PC. Nano Lett 2006;6:1202–1206. [PubMed: 16771580]

(35). McNeill CR, Watts B, Thomsen L, Belcher WJ, Kilcoyne ALD, Greenham NC, Dastoor PC. Small 2006;2:1432–1435. [PubMed: 17193000]

(36). Chehimi MM, Abel M-L, Perruchot C, Delamar M, Lascelles SF, Armes SP. Synth. Met 1999;104:51–59.

(37). Chattopadhyay S, Meredith JC. Macromol. Rapid Commun 2004;25:275–279.

(38). Niggemann M, Glatthaar M, Gombert A, Hinsch A, Wittwer V. Thin Solid Films 2004;451-452:619–623.

(39). Roman LS, Inganäs O, Granlund T, Nyberg T, Svensson M, Andersson MR, Hummelen JC. Adv. Mater 2000;12:189–195.

(40). Klimov E, Li W, Yang X, Hoffmann GG, Loos J. Macromolecules 2006;39:4493–4496.

(41). Perzon E, Zhang F, Andersson M, Mammo W, Inganäs O, Andersson MR. Adv. Mater 2007;19:3308–3311.

(42). Mammo W, Admassie S, Gadisa A, Zhang F, Inganas O, Andersson MR. Solar Energy Materials & Solar Cells 2007;91:1010–1018.

(43). Daoulas KC, Müller M, Stoykovich MP, Kang H, de Pablo JJ, Nealey PF. Langmuir 2008;24:1284–1295. [PubMed: 18067336]

(44). Li L, Lu G, Yang XJ. Mater. Chem 2008;18:1984.

(45). Berson S, Bettignies RD, Bailly S, Guillerez S. Adv. Funct. Mater 2007;17:1377–1384.

(46). Xin H, Kim FS, Jenekhe SA. J. Am. Chem. Soc 2008;130:5424–5425. [PubMed: 18376831]

(47). Moulé AJ, Meerholz K. Adv. Mater 2008;20:240–245.

(48). Na S-I, Kim S-S, Kwon S-S, Jo J, Kim J, Lee T, Kima D-Y. Appl. Phys. Lett 2007;91:173509.

(49). Becker H, Spreitzer H, Ibrom K, Kreuder W. Macromolecules 1999;32:4925–4932.

(50). Isobe H, Tanaka T, Nakanishi W, Lemiègre L, Nakamura EJ. Org. Chem 2005;70:4826–4832.

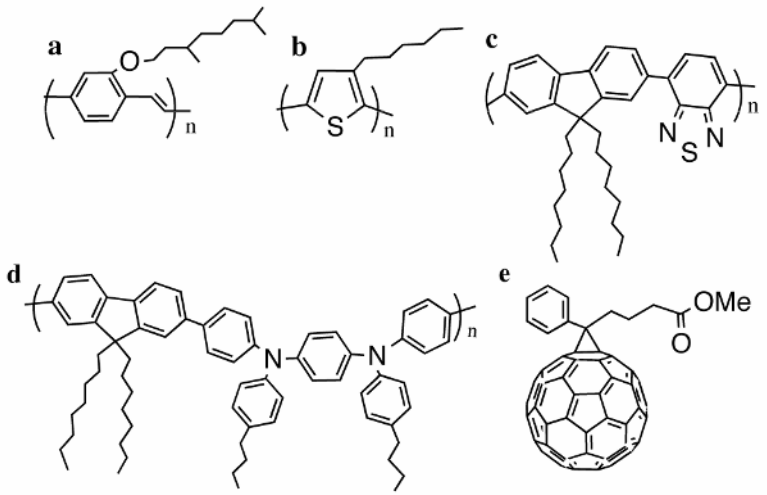

Figure 1.
Structures of donor and acceptor species used in this study: a) poly-[2-(3,7-dimethyloctyloxy)-5-methoxy-p-phenylenevinylene] (MDMO-PPV), b) poly-3-hexylthiophene (P3HT), c) poly[(9,9-dioctylflorenyl-2,7-diyl)-*co*-benzothiadiazole)] (F8BT), d) poly(9,9-dioctylfluorene-co-bis-N,N'-(4-butylphenyl)-bis-N,N'-phenyl-1,4-phenylendiamine) (PFB), and e) [6,6]-phenyl-C_{61}-butyric acid methyl ester (PCBM).

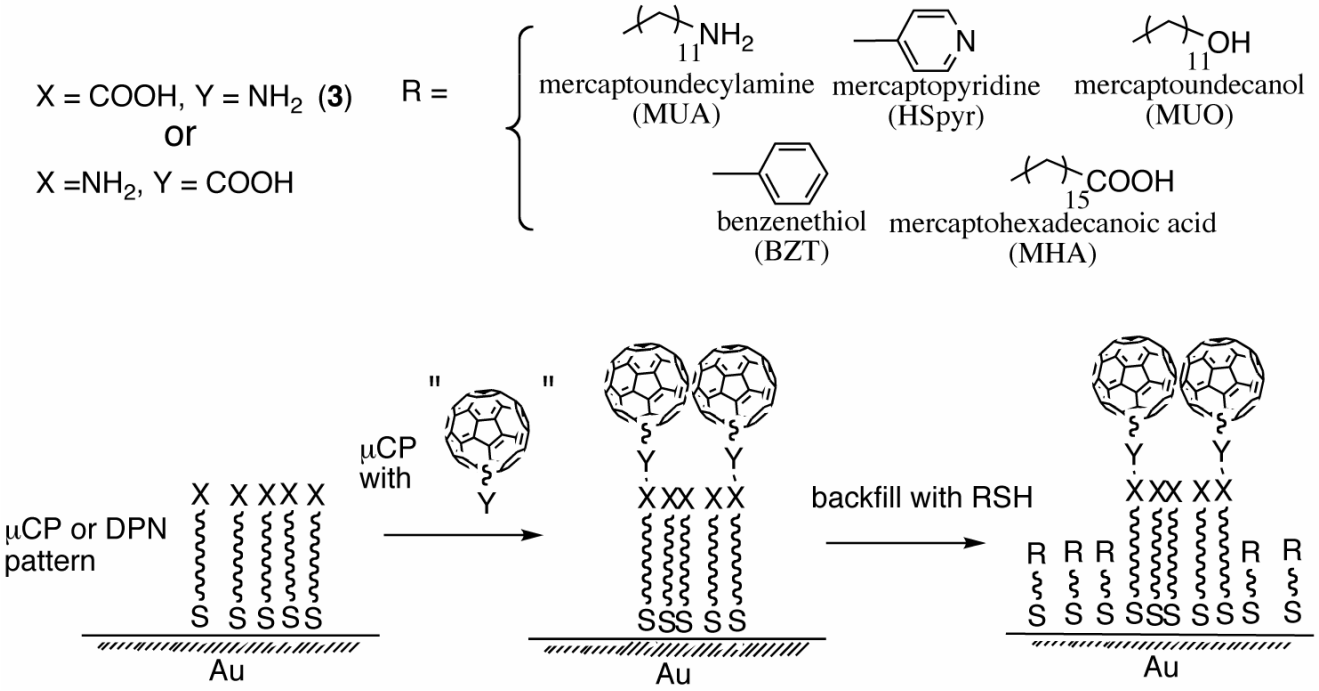

Figure 2.

Surface patterning method used to generate C_{60} patterns. The initial pattern is created by transferring MHA (or MUAm) to a bare gold surface via μCP or DPN. The fullerene functionality is then introduced onto the surface by μCP with **3** (or fullerene carboxylic acid) using a blank (featureless) PDMS stamp. Finally the rest of the surface is backfilled by immersing the substrate in a solution of one of the other thiols indicated.

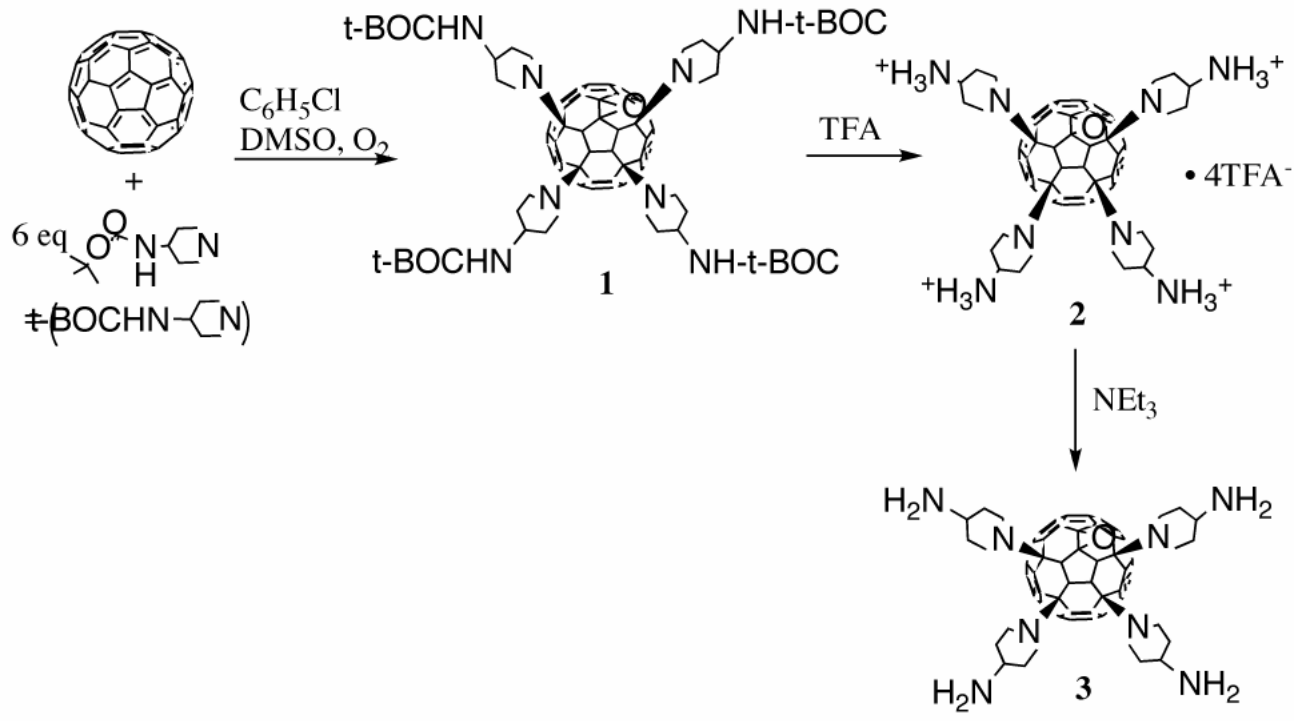

Scheme 1.
Synthesis of 3

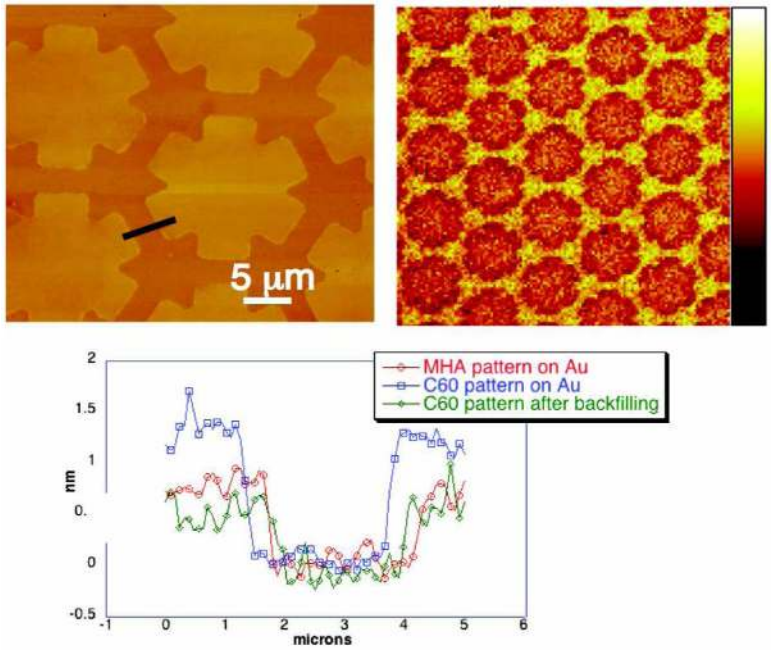

Figure 3.

(a) AFM topography image of an Au surface microcontact printed with MHA using the same PDMS stamp (b) ToF-SIMS map (using PCA) of C_{60}^+ ions generated from surface patterned as depicted in Figure 2, using a PDMS stamp consisting of a hexagonal array of star shaped posts (backfill HSpyr); regions giving rise to a higher concentration of C_{60}^+ ions are shown in darker colors (c) sequential height traces across the region indicated by black line in (a) after microcontact printing bare Au with MHA, after microcontaact printing the MHA-patterned surface with a featureless PDMS stamp inked with **3**, and after backfilling the now C_{60}-patterned surface with MUAm.

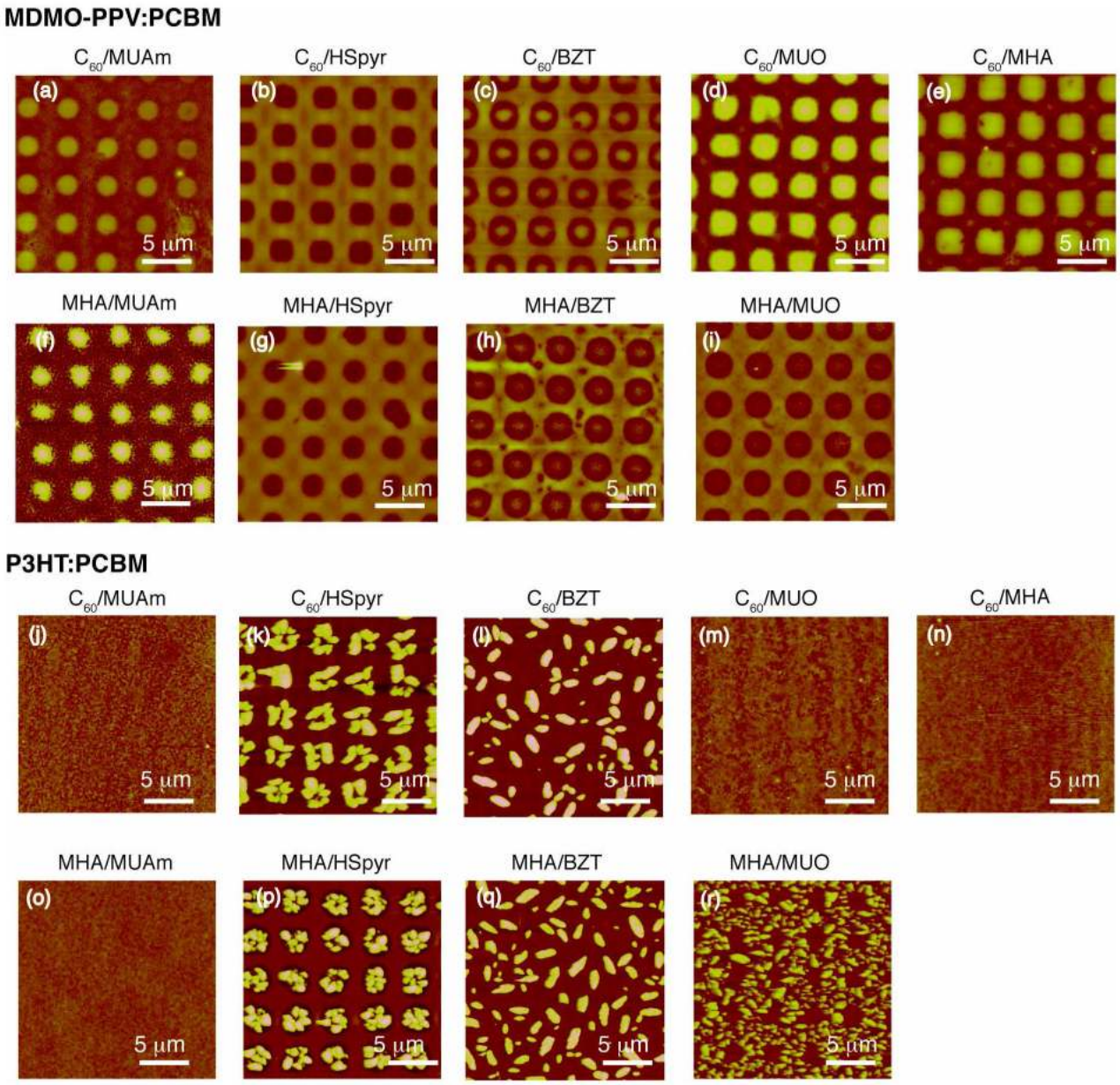

Figure 4.

AFM topography images (AC mode) for MDMO-PPV:PCBM and P3HT:PCBM films spin-coated onto pattern/backfill combinations, then annealed. MDMO-PPV films were ~100 nm thick before annealing; vertical (z) scales are (a)-(e), (g) 200 nm; (f), (h), (i) 100 nm. P3HT:PCBM films were ~ 60 nm thick before annealing; vertical (z) scales: (j), (m)-(o) 25 nm; and for (k), (l), (p)-(r) 200 nm.

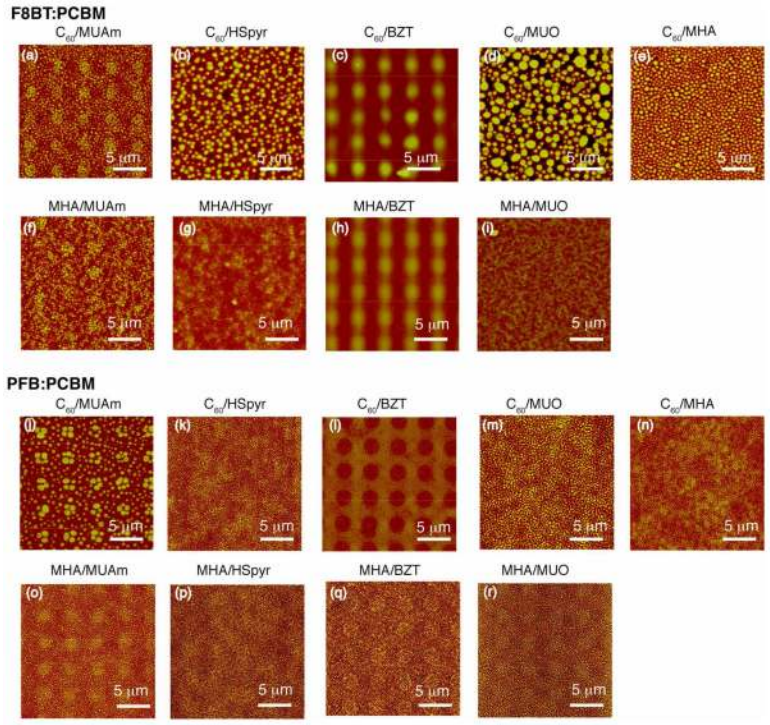

Figure 5.

AFM topography images (AC mode) for F8BT:PCBM and PFB:PCBM films spin-coated onto pattern/backfill combinations. Films were ~ 150 nm thick before annealing. The vertical (z) scales for the F8BT:PCBM samples are: (a)-(i) 200 nm. Vertical (z) scales for the PFB:PCBM samples: (j), (l) 100 nm; and for (k), (m)-(r) 25 nm.

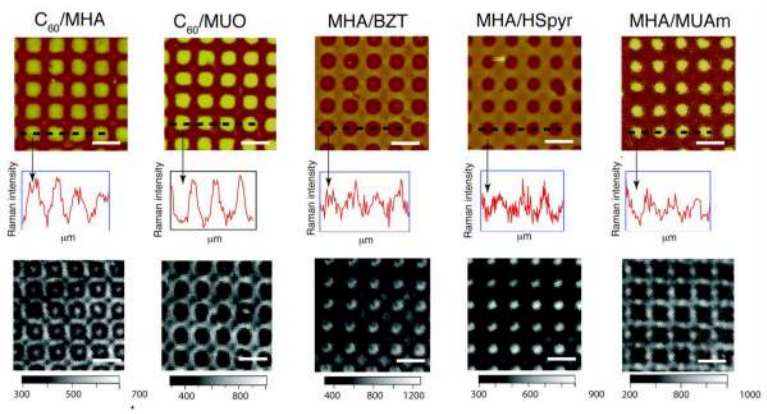

Figure 6.

Comparison of AFM topography (top row), Raman line scans (middle row) of peak intensity (cps) at 1460 cm^{-1} across regions indicated by the black dashed lines in the AFM images, and fluorescence images (bottom row) resulting from excitation at λ = 632 nm (exposure time = 0.2 sec) for MDMO:PPV:PCBM films prepared and annealed in the usual way on (a) C_{60}/MHA (b) C_{60}/MUO (c) MHA/BZT (d) MHA/HSpyr (e) MHA/MUAm patterned substrates. The black arrows indicates the center of a circle in the AFM image and the corresponding position in the Raman line scan; lateral scales of all images are equivalent, with scale bars = 5 μm. Vertical scale for a, b, e: 200 nm; for c, d: 100 nm.

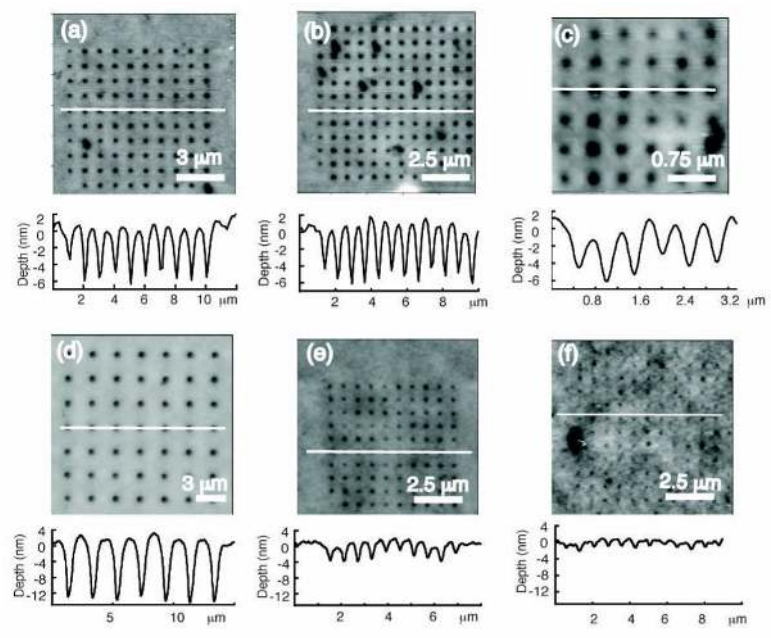

Figure 7.

AFM topography images (AC mode) and height profiles (across the regions indicated by white lines) for MDMO-PPV:PCBM films (after annealing) cast onto MHA/HSpyr DPN-patterned surfaces. In (a)-(c): the center-to-center pitch between ~200 nm diameter dots is varied (a) 1 μm , (b) 0.75 μm, (c) 0.5 μm. In (d)-(f): the pitch between the patterned dots is held constant at 0.75 μm while the diameter of the patterned dot is varied (d) 400 nm, (e) 200 nm, (f) 130 nm.

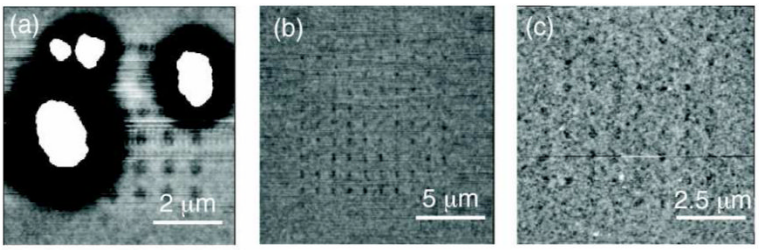

Figure 8.
AFM topography images (AC mode) for P3HT:PCBM films cast onto MHA/HSpyr DPN-patterned surfaces. (a) 600 nm dots with a center-to-center pitch of 1 μm, annealed at 125 °C for 30 minutes. The growth of large PCBM aggregates obscures much of the pattern. (b) 200 nm dots with a pitch of 1 mm, annealed at 125 °C for 30 minutes (c) 600 μm dots, with a pitch of 1 μm annealed at 120 °C, 30 minutes, then at 125 °C for 30 minutes.

Table 1

Summary of surface chemistries and polymer:PCBM films studied.

Surface chemistries (Pattern/backfill)[a]		Polymer:PCBM (w:w) (solvent; annealing conditions)
C_{60}/MUA	MHA/MUAm	MDMO-PPV:PCMB (1:4) (chlorobenzene; 80 °C, 8 hours)
m		
C_{60}/HSpyr	MHA /HSpyr	P3HT:PCBM (1:2) (chlorobenzene; 130 °C, 30 minutes)
C_{60}/BZT	MHA /BZT	F8BT: PCBM (1:2) (chloroform; 100 °C, 1 hour)
C_{60}/MUO	MHA /MUO	PFB:PCBM (1:2) (chloroform; 100 °C, 1 hour)
C_{60}/MHA		

[a] Pattern/backfill combinations were prepared as depicted in Figure 2. Except where indicated in the text, the patterns were prepared via microcontact printing using PDMS stamps consisting of square arrays of either 2.0 or 2.2 μm round posts with a 4 μm pitch.